Silver columnar thin films based half wavelength antennas for bright, directional emission from nanodiamond nitrogen-vacancy centers

Rajesh Kumar[1]*, Faraz A. Inam[2]*, Anh Ly[3], Carlo Bradac[3], S. Anantha Ramakrishna[1]
[1]*Department of Physics, Indian Institute of Technology Kanpur, Kanpur 208016, India* [2]*Deptartment of Physics, Aligarh Muslim University, Aligarh-202002, India* [3]*School of Mathematical and Physical Sciences, University of Technology Sydney, Ultimo NSW 2007, Australia**

Nitrogen-vacancy (NV) centers in nanodiamond (ND) are promising single photon source candidate for quantum technology. However, the poor NV emission rate and low outcoupling of light significantly hinder their effective use in practical implementations. To overcome this limit, we place NDs hosting NV centers on silver columnar thin films (CTFs) and measure an increase in emittance by an order of magnitude. The CTFs consist of silver nanocolumns whose length was chosen to be half the wavelength of the emitted light. The silver nanocolumns act as efficient optical antennas that couple to the NV centers via the optical near-field and outcouple the excitation energy of the NV centers effectively into the optical far-field. A large distribution of radiated powers from different NDs is observed. Computer simulations show this distribution to arise from the different orientations of the emitting dipoles with respect to the columnar axis. We also report that further structuring of the silver CTF into gratings yields higher photon emission.

I. INTRODUCTION

Single photons sources are one of the most critical components of quantum information processing[1] and quantum cryptography[2]. The desirable requirements for single photon sources include stable emission, high photoemission rate and, ideally, angularly-confined emission[3]. Nitrogen-vacancy (NV) centers in nanodiamond (ND) are promising single photon source candidates as they possess stable emission even at room temperature[4]. They are, however, limited by a long radiative lifetime due to poor index matching at the diamond-air interface, which results in low emission rates[5]. Several methods have been suggested to outcouple the emission more efficiently for instance via coating with higher refractive index materials[6,7], near-field coupling to plasmonic and photonic structures[5,8–12], waveguides[13–15], tapered optical fibers[16] and fiber tips[17]. Also, anisotropic metamaterials[18] with hyperbolic dispersion have been used as they have divergent photonic localised density of states (LDOS) which can enhance the emission of NV centers in NDs[19].

Atoms and molecules are very inefficient emitters due to their sub-wavelength small size[20]. Embedding them in a larger scattering structure such as a spherical nanodiamond can increase the spontaneous emission intensity. Nevertheless, diamond nanoparticles can also be sub-wavelength in size, which intrinsically inhibits large-scale enhancement. The impedance mismatch due to the large refractive index of diamond also hinders the NV emission. Further, the radiation pattern of a small spherical nanoparticle is typically dipole-like[21] and does not display sufficient angular selectivity. In this context, a linear antenna of length (l) smaller than the wavelength can emit radiation proportional to $(l/\lambda)^3$ (the Wheeler limit)[22]. The antenna geometry critically determines the emission rate and radiation pattern and its length can severely impact the radiation. To produce large emission the ideal length of an antenna should be about half the wavelength($\lambda/2$) of the emitted light. Thus, it would be desirable to couple the NV in ND to ($\lambda/2$)-sized antennas in the near-field to create enhanced outcoupling of the emission, as well as to provide directional output.

In this work, we place NDs hosting NV centers in silver columnar thin films (CTFs). We find that the NV emittance (measured photon count rates) is enhanced by about an order of magnitude when the CTF nano-column length is about 350 nm (approximately half the wavelength of the central peak of the NV emission spectrum ∼680 nm). The silver CTF consists of an anisotropic dielectric medium with hyperbolic dispersion[23]. By numerical simulations the nanodiamond NV is treated as a dipole emitter embedded in the nanostructured columnar medium we find that the emittance is enhanced due to the nanocolumns acting as efficient optical antennas. The emittance from a large set of nanodiamond emitters in CTF was measured by confocal microscopy. The study revealed a wide distribution of measured photon count rates from NV centers on a given substrate[24]. The presence of the silver nanocolumns shifts the entire measured count rate distribution to higher values with increased mean and median by roughly one order of magnitude. Detailed simulations reveal that similar distributions arise due to the different orientations of the emitting dipole in the ND with respect to the nanocolumn axis and the consequent difference in coupling. Further structuring of the silver CTF into grating structures resulted in marginal enhancement in the measured count rates as compared to that for the unpatterned CTF. Occasionally, emitters with relatively higher measured count rates were observed on the CTF gratings. These studies

* Both authors contributed equally.
kraj@iitk.ac.in, faraz.inam.phy@amu.ac.in

demonstrate the enormous potential of plasmonic CTF for developing efficient sources using NV centers in ND.

II. SAMPLE PREPARATION

Silver columnar thin films (CTF) were deposited on glass (fused silica) and silicon substrates with and without photoresist gratings by evaporation of silver at large oblique angles. The one-dimensional gratings of photoresist (ma-P 1205) were made by Laser Interference Lithography (LIL)[25] at a 442-nm wavelength over an area of about 30 mm^2. 1-D gratings with pitches of 500 nm, 600 nm, 700 nm and 800 nm were prepared. Gratings of different periodicity were used as substrates to deposit the CTFs. A collimated flux of silver was directed onto the substrate, cooled by a Peltier cooler to about -20°C, at an angle of 80° with respect to the substrate normal in a vacuum of 5×10^{-6} mbar. Random nucleation sites were formed in the initial film growth which, by shadowing the regions behind them, resulted in the columnar morphology of the thin film[26]. The deposition rate was maintained at 15-19 $\mathring{A}$/s and monitored using a quartz crystal monitor. Oblique angle deposition of a collimated flux of silver vapour on flat silicon-(100) substrates yielded forests of randomly distributed but highly oriented nanocolumns of silver as shown in Fig. 1(a). Comparatively, deposition on linear gratings of a polymer yielded a periodic array of oriented nanocolumns as shown in Fig. 1(b). The nanocolumns have diameters of (40±5) nm and length of about (350±10) nm. It is apparent from the cross-sectional view in the inset of Fig 1(b) that the nanocolumns grow uniformly only from the ridges of the grating. We also note that some of the nanocolumns merge into one another due to the finite collimation of the silver vapour as well as the finite deposition rate [26]. Regardless, the variation in column diameter is minor and the nanocolumn alignment is uniform across the sample. Notably, the tilt of the nanocolumns with respect to the substrate, the length of the nanocolumns, and the density and period of the grating are all variables that can be optimised to maximise the emission from the nanodiamond NV centers.

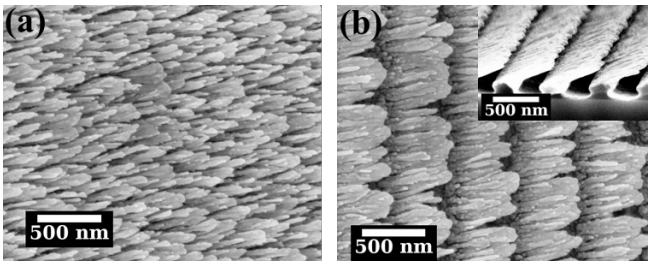

FIG. 1. a) Top view of field-effect scanning electron microscopy (FESEM) image of Ag CTF on silicon substrate. b) Top view of FESEM image of Ag CTF on 500-nm PR grating. The inset shows the cross-sectional view.

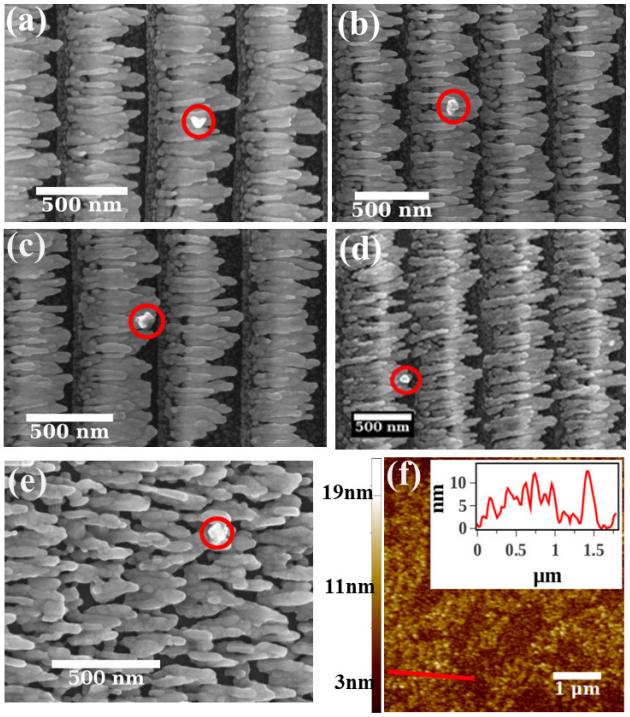

FIG. 2. Top view of FESEM image of ND deposited on 500-nm periodicity silver CTF on three different locations (a), (b) and (c), 600-nm periodic silver CTF (d) unpatterned silver CTF (e). (f) Atomic force microscopy (AFM) image of the surface topography of the silver film coated sample, over an area of 5 μm × 5 μm; the inset shows the line profile of the film.

Plain silver films were also deposited on the glass substrate and on photoresist gratings with different pitches by physical vapour deposition at normal incidence. A flux of silver in vacuum at 7×10^{-6} mbar was normally directed on the samples at a low deposition rate 0.7-1.5 $\mathring{A}$/s. A 25-μL aqueous solution of NDs was spin coated on silver CTF samples and the glass substrate at 3000 rpm, for 1 minute. The same conditions were used for all the samples.

III. CHARACTERIZATION AND MEASUREMENT

The fabricated CTF samples were imaged using field-effect scanning electron microscopy (FESEM) (BP 40 SUPRA Carl Zeiss instruments). 2 shows the top view of the FESEM image of nanodiamonds deposited on different silver CTF samples. The NDs are highlighted by a red circle. The images show that the NDs are located on the tip of the silver CTF and that they are also isolated from others NDs. It is evident from the FESEM images that the morphology of silver CTF does not change or get damaged by spin coating the solution of NDs on top.

An atomic force microscope (XE70, Park System,

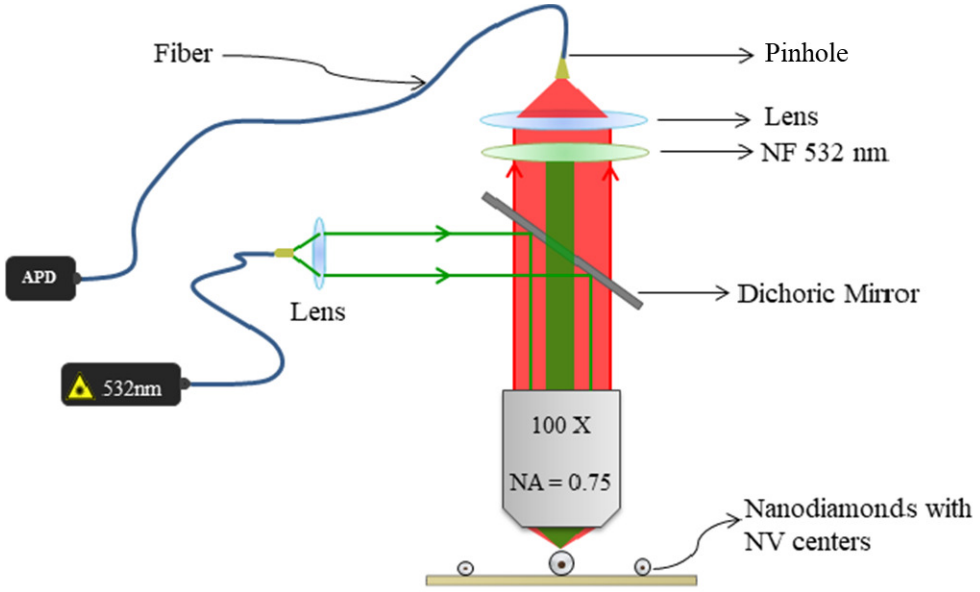

FIG. 3. Schematic diagram of the experimental setup of the confocal fluorescence microscope. NF 532 nm − notch filter to cut off the 532-nm excitation light. APD − avalanche photodiode.

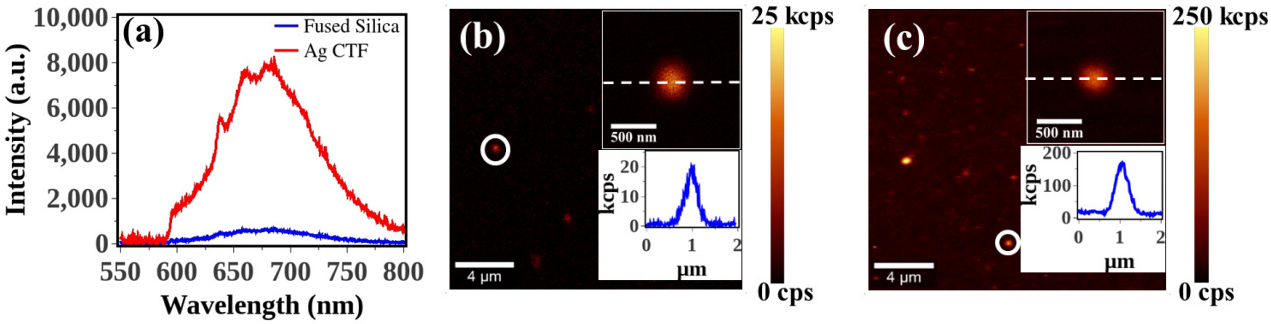

FIG. 4. a) NV centers spectrum obtained from our ND samples, at room temperature. b, c) Confocal images of the fluorescence emission from ND-NV centers over an area of 20 μm × 20 μm on a glass substrate (b) and when placed on the Ag CTF 500-nm grating sample (c). The confocal scan of a single emitting ND is shown in the top inset of both Figs. over an area of 2 μm × 2 μm. The bottom inset shows the image intensity along the dashed line.

South Korea) was used to determine the grating period and surface topography of the different samples. Figure 2(f) shows the surface topography of a plane silver film on the glass substrate. The film has a typical rms roughness of $\sim$ 3.5 nm, as measured from the line profile in the inset of Fig 2(f).

Optical characterizations were performed using a commercial confocal microscope (WITec, alpha300 S). The schematic diagram of the experimental setup of the confocal fluorescence microscope is shown in Fig 3. A 532-nm continuous-wave (CW) diode laser was used to excite the NV centers in NDs. The laser beam was coupled to the microscope by a single-mode optical fiber. A 100× objective with a numerical aperture (NA) of 0.75 was used to focus the light onto the sample. Fluorescence was collected from the NDs using the same objective through a 532-nm notch filter and directed to an avalanche photodiode (APD) for detection in photon-counting mode. Lifetime measurements of the ND-NVs were carried out using a lab-built confocal microscope with a 100× objective and a 0.9 NA, and a Fianium WhiteLase excitation laser source (532 nm wavelength, 10 MHz repetition rate, 10 μW excitation power).

The NV emission spectrum from a nanodiamond on a glass substrate and on Ag CTF sample is shown in Fig. 4(a), which clearly shows the zero phonon line (ZPL) at 637 nm, along with the typical broad phonon sideband at higher wavelengths. The fluorescence confocal images of the emission from NV centers in NDs on a glass substrate, and on a 500-nm Ag CTF grating are

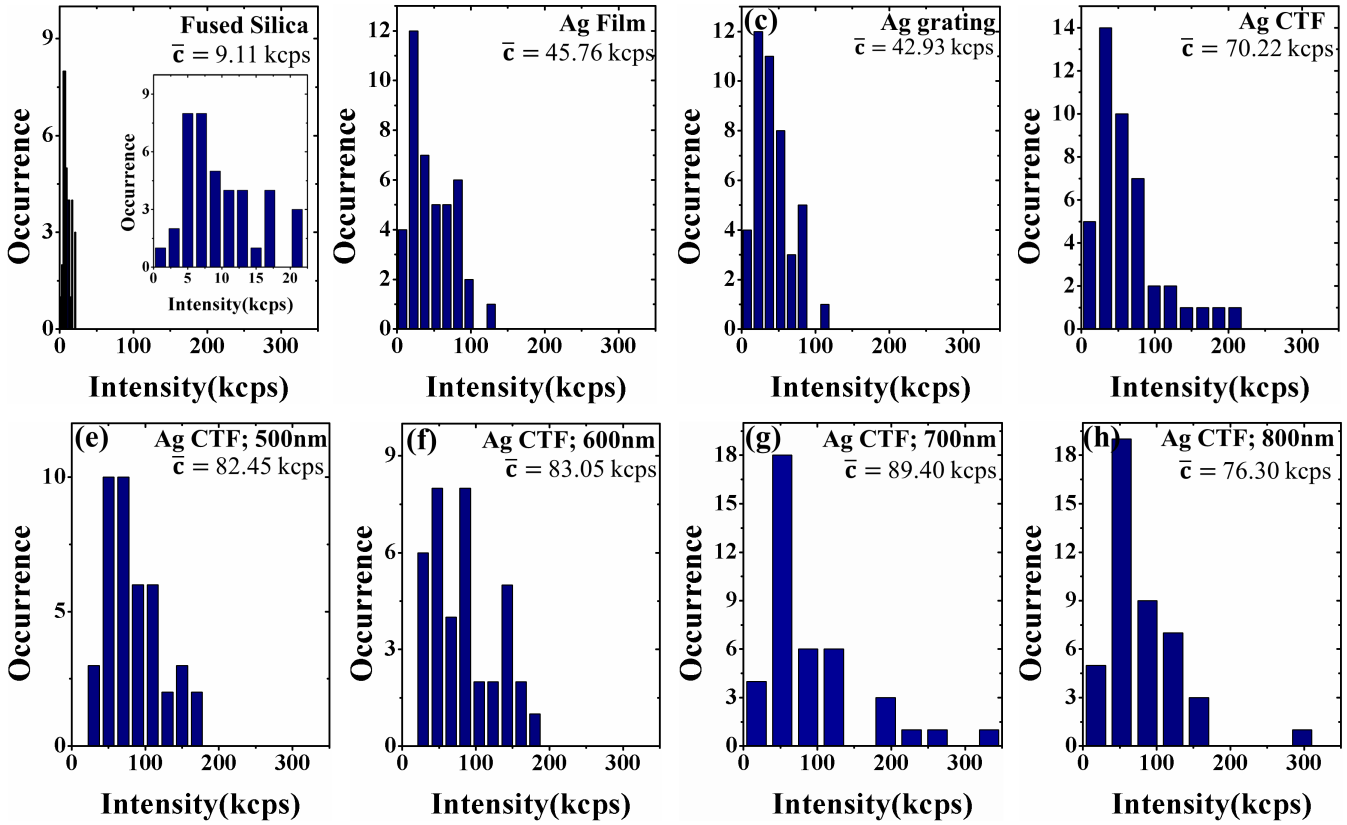

FIG. 5. Statistical distribution of the experimentally measured powers from NV centers in ND placed on different surfaces: on a glass substrate (a), on a plain silver film (b), on 600-nm silver grating (c), on unpatterned silver CTF (d), and on periodically patterned silver CTF with the period from 500 nm to 800 nm (e–h), respectively. $\bar{c}$ − mean value.

shown in Fig 4(b) and 4(c), respectively. While some clusters of emitting NDs were present, only isolated centers with a diffraction-limited fluorescence spot [see inset in Figs. 4(b) and 4(c)] were considered in the photoemission measurements. The scanning electron microscope (SEM) images of the nanodiamonds on CTF samples show that most of the diamond nanocrystals are located near the top-end of the nanocolumns (Fig.2). By measuring the NV center photon count rates, the emission from the individual NV-ND on Ag CTF is found to be typically enhanced by over an order of magnitude compared to the NV emission from ND on the glass substrate—used as the reference control sample. A wide distribution in the NV center collected photon count rates on both the glass substrate and the CTF-sample was observed and attributed to the arbitrary orientation and location of the NV dipole within the diamond crystal[6]. A statistical study of the NV center emission on glass and various CTF substrates was carried out to measure the average influence of the different substrates on the NV center emission. For this, around 40 stable near-diffraction-limited emitters were studied on various substrates. The limited number of studied emitters may not result in a proper normalized distribution, however the mean will vary only within the measured standard deviation. The distributions of the measured photon count rates from the NDs on various substrates are plotted in Fig. 5.

The emission from NDs on glass shows a broad distribution of measured count rates ranging from 0 to 20 kcps with a mean of (9 ± 5) kcps and a mode of 5 kcps. For the NDs placed on the unpatterned silver film, the mean increases to about (46 ± 29) kcps, the mode to about 20 kcps, and there are a few centers with large count rates around 100 kcps. This enhancement is expected due to the plasmonic nature of the silver film as well as the surface roughness, and it is comparable to previous reports for other emitters[27–29]. The structuring of the silver CTF into a grating-like structure does not seem to affect the distribution of emissions in a notable way. When the NDs are deposited on a silver CTF, larger enhancements are observed, with the mean of the measured count rates increasing to up to (70 ± 53) kcps and the mode to 40 kcps—with measured count rates of up to 200 kcps from some emitters. Structuring the CTF further into a grating causes some of the embedded NDs to display even higher count rates. While the mean and the mode increase by only about 10%, NV cen-

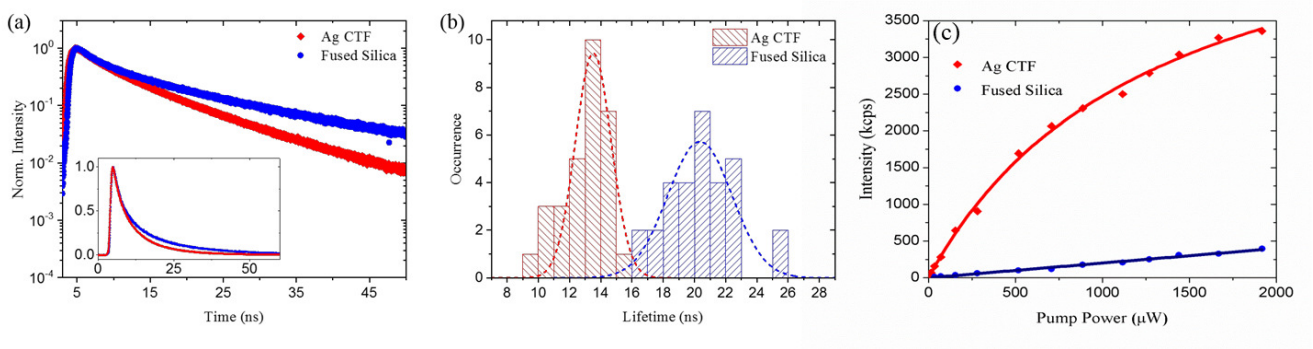

FIG. 6. a) Lifetime decay curves for NV centers emission on Ag CTF (red) and glass (blue) substrates. b) Corresponding lifetime distributions for NV center emission on the two substrates. The average lifetime values are $\tau = (13.5 \pm 2.5)$ ns for the Ag CTF sample and $\tau = (20.4 \pm 4.8)$ ns for the glass sample, respectively. (c) Emission intensity saturation curve for a nanodiamond on silver CTF (red) and for a reference nanodiamond on glass (glass) substrate (blue).

ters with very large measured count rates of up to and above 300 kcps were observed. These occurrences are, however, infrequent and probably arise due to cavity-like resonances in the grating as discussed below. Whilst we observed a wide distribution of measured count rates in all cases, the distributions appear consistent within each sample, indicating a possible common origin. We attribute the distribution of measured count rates and, in turn, of the emission rates to the different orientation of the radiating dipoles (NVs) relative to the substrate and the nanocolumnar axis.

A measure of the dipole emitter's total decay rate enhancement can be determined by measuring the corresponding reduction in the emitter's lifetime. Figure 6 (b) shows the distribution of measured lifetimes for nanodiamond NV centers on Ag CTF and glass substrates. The results show the mean NV center lifetime on Ag CTF substrates to be nearly half [$\tau = (13.5 \pm 2.5)$ ns] the value on the glass substrate [$\tau = (20.4 \pm 4.8)$ ns]. This corresponds to an enhancement in the NV centers total decay rate by roughly a factor of 2. The observed enhancement by one order of magnitude in photon count rates is therefore likely the result of the Ag CTF nanocolumn antenna effect of directing the NV emission mainly towards the top, i.e. orthogonal with respect to the substrate plane.

NV center lifetime in bulk diamond is well-known to be constant around 11.6 ns[30,31] due to a homogenous electrodynamic environment for all NV dipole orientations in the bulk diamond. However, in subwavelength size nanodiamond crystals, NV centers are known to have a large distribution in the emission lifetimes range from about 5 - 50 ns with mean about 22 - 23 ns[6,32,33]. The distribution results from various factors including the NV dipoles proximity and its orientation relative to the air-glass (substrate)[6,34,35], the irregularity in the crystal geometry for crystal sizes in the subwavelength regime[6,33] as well as due to the large distribution in the quantum efficiencies of individual NV centers in the ND[24,36]. For NV dipoles with variable quantum efficiencies, the suppression in the local density of states (LDOS) due to Lorentz-Lorenz effect[37] in subwavelength, highly dielectric diamond crystals will also show a significant variation[36,38], leading to a large distribution of the emission rates.

Fluorescence counts from photostable single nanodiamond deposited on silver CTF and glass were measured as a function of different incident powers of a 532-nm continuous-wave diode laser. The power saturation of the nanodiamond emission with respect to the incident excitation power, when placed on silver CTF and glass (glass), is shown in Fig. 6(c). Here the power shown on the x-axis of the graph is the excitation laser power measured at the output-end of the single mode optical fiber just before coupling to the back of the microscope objective. A neutral density filter is placed in the collection to avoid the saturation of the avalanche photodiode (APD) detector. So the measured photon count rates shown in Fig. 6(c) are relative. The measured photon count rates increase almost by an order of magnitude, in the case of the silver CTF sample as compared to the NV centers emission on the glass substrate. The NV emission of silver CTF also appears to reach the saturation level at a lower power compared to the case of its emission on the reference glass substrate. This may result from the localization of the excitation laser (532 nm) scattered field at the NV dipole location due to the silver CTF.

The one-order-of-magnitude increase in the measured photon count rates indicates that the half-wavelength Ag CTF nanocolumns are acting as efficient antennas which direct the dipole radiated power along the top direction. The effectiveness of the half-wavelength Ag CTF nanocolumn antennas can also be seen from the collected NV emission spectrum [Fig. 4(a)] on glass and CTF substrates, as well as from the power saturation curves of the NV emission on glass and CTF substrates [Fig. 6(c)]. In all these cases, an enhancement of about an order of magnitude in the NV center emission is observed.

For the completeness of our study, we also performed auto-correlation studies on the NV centers on various

substrates. However, as our NDs were irradiated, we could not observe any anti-bunching behavior from these ND based NV centers due to the presence of multiple NVs in each crystal. Since we used the same ND solution for all substrates including the glass, Ag film and Ag CTFs, we expect the substrate influence should remain the same even in the case of multiple NV centers. Also a multi-exponential decay behavior can be observed in the NV center lifetime curves on different substrates 6. As discussed above, individual NV dipoles are expected to different lifetimes due the difference in its dipole orientations relative to the air-glass interface of the substrate[34]. Also its proximity to the interface will have an influence on its lifetime[34]. The individual quantum efficiency of these emitters is also expected to be different[24]. Since we couldn't observe any substantial dip in the auto-correlation curves, many NV centers are expected to be present in each individual crystal. The lifetime decay curves are therefore expected to have a multi-exponential behavior. Through numerical calculations we have checked and verified that fitting a multi-exponential curve by a single exponential fit, we get lifetimes close to the average lifetime of all the individual centers. Since, we have observed continuity in the NV decay curve fittings for the various substrates, we expect the average lifetime values to remains the nearly the same in each case.

IV. NUMERICAL CALCULATIONS

A detailed computational study of the emission originating from a point electric dipole (NV center) in the ND, placed on various structures, was carried out using the finite element method implemented in the COMSOL Multiphysics® suite. The ND was taken to be a spherical particle with a diameter of 45 nm and refractive index of 2.47. The silver CTF was modeled as an array of silver prolate ellipsoids inclined at 25^0 on a dielectric substrate (photoresist with a refractive index of 1.62). The Lorentz-Drude model was used to describe the dielectric permittivity of silver with plasma frequency of 2180 THz and damping of 5.0778 THz[39]. Clumps of two or three nanocolumns on the grating ridge were considered in a unit cell, similar to the FESEM images in Fig. 1. Geometrical parameters of CTF were obtained from the cross-sectional FESEM image shown in Fig. 1(b), i.e. length: (350 nm ± 10) nm and diameter: (40 nm ± 5) nm. Floquet boundary conditions were used in the y-direction, and perfect matching layer (PML) was used at the boundaries along the x-direction. The distance between two nanocolumns along the y-direction was considered to be 5 nm. The nanocolumnar axis was set to lie in the XZ-plane. The drive frequency of the dipole source corresponds to the peak emission wavelength, 680 nm.

A. Length optimization

The nanocolumnar length was optimized numerically to obtain maximum emission rates. The effect on the coupling of the emission due to the orientation of the dipoles with respect to the nanocolumns was also analyzed. The nanodiamonds were considered to be at the tip of the nanocolumn. To have a comparison of the measured power for the nanodiamond NV center emission on various substrates, the power radiated by the point electric dipole in the upward direction was calculated by integrating the z-component of the time-averaged Poynting vector flux over a flat surface at 300 nm above the dipole. Figure 7(a) shows the dipole radiated powers on the top surface for different nanocolumnar lengths corresponding to the three perpendicular dipole orientations. The nanocolumnar diameter was considered to be 45 nm. There is a large variation in the emission rate near about the 400 nm length of the nanocolumn when the dipole is oriented along the z-direction. The emission rate is also close to the maximum value at the 400-nm value for the length of the nanocolumn for the dipole orientation along the x- and y-directions. The emission rates are large for nanocolumnar length in the range 350-450 nm.

The simple Ag nanocolumns used here are essentially a form of dipole antenna, the antenna modes being dipolar resonances[40]. The coupling of the dipole radiation fields to the antenna modes should be sensitive to the dipole orientation relative to Ag antenna. For effective coupling, the wave-vectors of the point-dipole radiation pattern should be matched with resonance modes the Ag nanocolumn antenna. This coupling is expected to be maximum for emitter dipole's orientation perpendicular to the Ag nanocolumn antenna surface. In this case, the wave-vectors of the emitter dipole's radiation field will be along the nanocolumn surface and will effectively couple to the radiation modes of the Ag nanocolumn dipole antenna. In Fig. 7(c), the top radiated power is calculated for the different dipole orientations in the XZ-plane. It can be observed from the figure that the maximum top radiated power is achieved when the dipole is oriented perpendicular to the nanocolumnar axis. Figure 7(d) shows the top radiated power from a point electric dipole in ND placed on a glass substrate for the different dipole orientations in the XZ-plane. In this case also, the maximum power is observed when the dipole orientation is perpendicular to the glass substrate. For a dipole oriented perpendicular to the interface are known to experience the highest spontaneous emission rates[34]. In the case, the air-glass interface itself is known to act as an antenna directing most of the radiated power along the vertical directions[41]. The same size for the unit cell was used in both cases for comparison.

Figure 7(e) shows the normalized scattered electric field close to the tip of the silver CTF nanorod as a function of the excitation wavelength. The p-polarized (electric field-vector along the glass surface) plane wave at normal incidence was used for excitation. The normal-

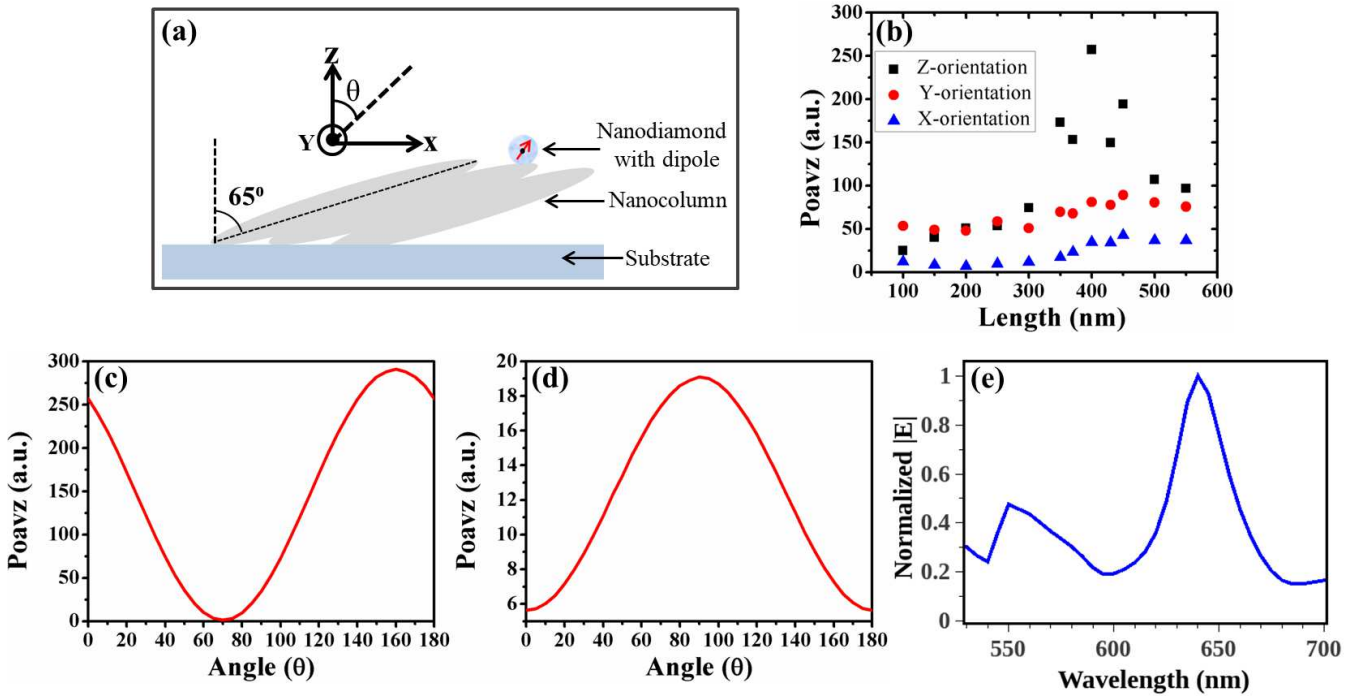

FIG. 7. a) Schematic diagram of silver CTF with ND on the tip of nanocolumn. (b)Top radiated power of point electric dipole in nanodiamond placed near the tip of nanocolumns with different length for three orthogonal dipole orientations. Top radiated power with respect to dipole orientation in the XZ-plane c) when the dipole was placed near the tip of nanocolumn with 400-nm length and d) when dipole placed on the glass substrate. (e) Absolute value of the normalized electric field as a function of wavelength calculated at a point close to the tip of the nanorod.

ized scattered electric field was calculated at the location of the point dipole in the nanodiamond. The Fig. shows that there are two resonances at 550 nm and 640 nm which are very close to the excitation field and the zero phonon line of the NV emission, respectively. This indicates that both the excitation field and the emission are enhanced due to the intense local electric field [12] of the silver CTF and the presence of the two broad resonance peaks.

B. Statistical study of the emission rates

We computationally performed a statistical study of the emission from the NV centers in ND on the different substrates. Dipoles with 100 different orientations and locations within the diamond nanocrystal were randomly chosen for the statistical study of the top radiated powers. The distribution of the calculated powers on different substrates are shown in Figs. 8(a)-(d), where a common unit cell size was used in all cases to enable direct comparison. To compare with the experimental measurements, the ratio of the experimental mean photon collection rate to the calculated mean power in the case of NDs on a glass substrate was used as a common factor to scale all the other calculated results. The range of top radiated powers calculated [Fig. 8(a)] for the glass substrate is about the same as experimentally measured [Fig. 5 (a)], suggesting that the distributions mainly arise due to the random orientations of the dipoles. The top radiated power distributions from the dipoles in ND on the silver film and on the 700-nm period silver grating, in Fig. 8(b) and 8(c), show that the top radiated power is enhanced, yet not as much as observed experimentally. The distribution of powers, however, appears similar in both cases. The limited enhancements are probably due to not taking into account the surface roughness of the silver in the calculations. The distribution of the radiated powers for the dipole in the ND on the silver CTF grating [Fig. 8(d)] is large and appears very similar to the powers measured experimentally [Fig. 5(h)]. Reassuringly, there are also rare cases where the measured power exceeds 300 kcps, with the mean and mode having values similar to the experiments [Fig. 5(h)].

C. Far Field Calculations

The electromagnetic fields and the power flow in the system offer an insight into the physical mechanism. Figure 9(a) shows the x-component of the electric field along with streamline plot of the Poynting vector field for the radiating dipole located at the top of the middle nanocolumn in a silver CTF. Figure 9(b) shows the same quan-

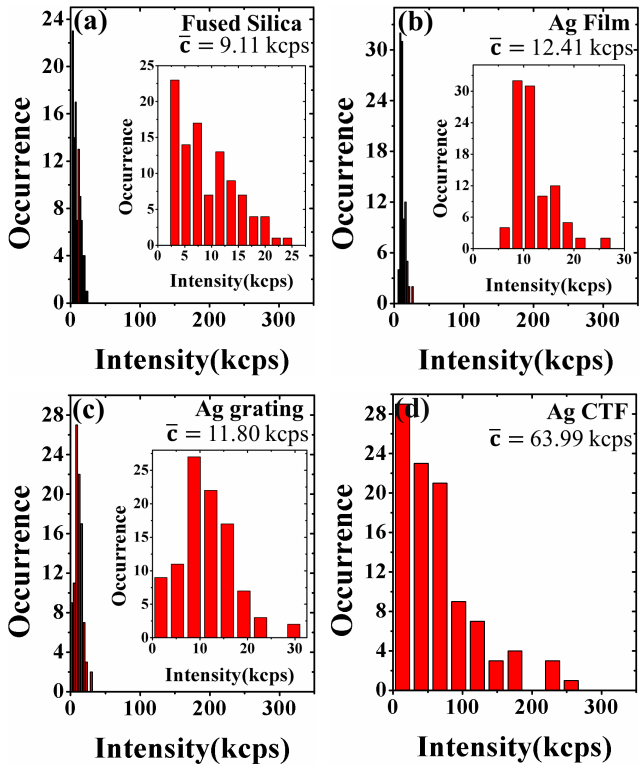

FIG. 8. Statistical distributions of the computed top radiated powers of a point dipole with a nanodiamond placed on different samples: a) on a glass substrate, b) on silver film, c) on a 700-nm silver grating, and d) on periodically-patterned Ag CTF with a period of 700 nm.

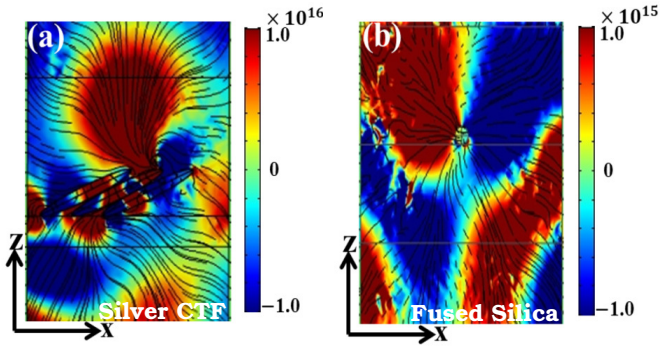

FIG. 9. a) Color plot of the x-component of the electric field along with streamlines showing the Poynting vector (power flow) of a radiating dipole in an ND sphere placed on the silver CTF. b) Corresponding quantities for the dipole in an ND placed on the glass substrate.

tities when the ND is placed on a glass substrate. In the case of Fig. 9(b) the radiation flow is more isotropic, although, the field is null in the normal direction due to the interference of the field emanating from the dipole and the reflected dipole. This is consistent with the radiation from a small-sized, dipole emitter[42]. When we look at the fields in the case of the dipole placed on the silver nanocolumns, we immediately note the presence of a resonant electromagnetic mode on the nanocolumns. These currents on the ($\lambda/2$)-sized nanocolumns radiate directionally as the Poynting vector maps clearly highlight. This directionality arises solely due to the strong coupling of the dipole fields to the nanocolumns in the near-field regime.

Polar plots of the far-field emission intensities for three orthogonal dipole orientations are shown in Fig. 10. Figures 10(a) and (b) show the polar plots of the far-field intensity in the YZ-plane when the dipole is placed on a glass substrate with orientation along the x- and z-directions, respectively. Figures 10(c) and (d) show the polar plots of the far-field intensity in the YZ- and XZ-planes when the dipole is placed on the tip of the nanocolumn with orientation along the x- and y-direction, respectively. The far-field radiation intensity pattern in the case of a dipole placed on the nanocolumn is quite different when the dipole is placed on the glass substrate. The main differences are that the emission is confined within a smaller angular range in the case of the dipole placed on the CTF and that the intensity is enhanced, particularly for dipole orientations along the y- and z-direction [Figs. 10(c) and (e)]. For the dipole orientation along the z-direction, there is an order of magnitude increase in the far-field intensity.

V. DISCUSSION

Overall, we observe that NV centers in NDs emit more efficiently and directionally in the presence of silver nanocolumns. The degree of enhancement is broad, which we attribute to the random spread of possible orientations of the dipole with respect to the nanocolumn axis. This evidence principally points to the fact that the nanocolumns act as efficient ($\lambda/2$) antennas driven in the near field by the excited NV center. To put these results into context, we made the following working assumptions. We considered the nanodiamond NV centers to be radiative and highly quantum efficient[43]. The average quantum efficiency of NV centers in NDs is known to vary among individual centres[24], with an average value of about 0.7 for similar sized ND crystals[33]. Since our confocal microscope is a commercial model not optimized for single photon counting studies and has a lower collection efficiency with the objective lens numerical aperture (NA) of 0.75 (the detection efficiency of our confocal system is expected to be about 1% for dipole emission on top of the glass substrate), we expect to collect light from only bright emitters with higher quantum efficiencies. Other works studying NV center spontaneous emission enhancement using plasmonic schemes have also considered the NVs to have high quantum efficiency[43]. As the NV centers are embedded within the NDs, and well protected, strong quenching effects due to the silver

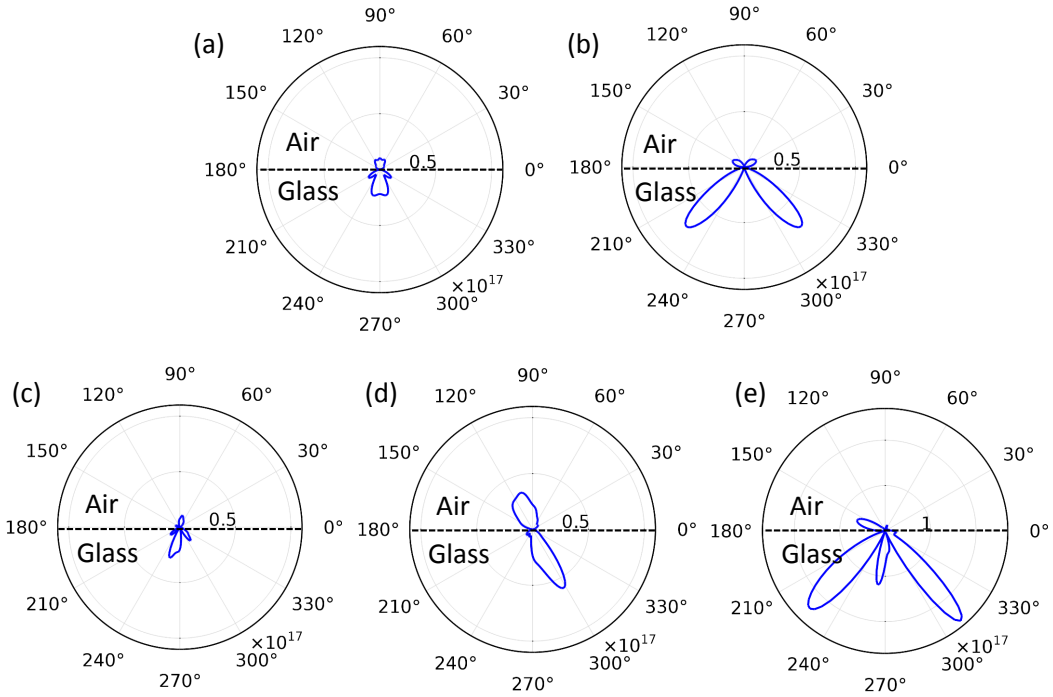

FIG. 10. Polar plots of far-field radiation intensity patterns: when an electric point dipole was placed on a glass substrate with orientation along the x-direction and z-direction, respectively (a, b); with orientations along the x-, y- and z-directions respectively when placed on the tip of nanocolumnar where nanorod was oriented in XZ-plane (c–e). For comparison, sub-figures (a) to (d) are plotted on the same scale. However, due to the relatively higher magnitude of radiation intensities for sub-figure (e), it is plotted on a higher scale.

nanostructure are unlikely and therefore was not considered in our analysis. While the enhancements in the case of NDs placed on the plane silver film are increased due the surface roughness, our simulations assume no surface roughness for the nanocolumns in case of ND placed on the CTF, explaining slight discrepancy between simulations and experiments. The emission from the NV coupled to the larger length scale ($\sim \lambda/2$) of the Ag CTF nanocolumns shows one-order-of-magnitude enhancement in the emittance. A good match between experiment and simulation results was found in this case. The surface roughness is expected to have minimal effects in this ($\sim \lambda/2$) length scale scenario. We thus attribute the effect seen here to the nanoantenna geometry rather than the surface roughness as in surface-enhanced fluorescence or surface-enhanced Raman scattering.

VI. CONCLUSIONS

We have measured a significant enhancement in the emission of NV centers in NDs placed on silver CTFs. The emittance is enhanced by about one order of magnitude compared to the emittance of nanodiamonds placed on a glass substrate. A wide variation of the measured photon count rates is shown to arise from the random orientation of the emitting dipoles with respect to the substrate or the silver nanocolumns. We show by computer simulations that the enhancement mainly arises from the coupling of the near-field radiation to the silver nanocolumns, which hence act as efficient antennas, approximately ($\lambda/2$) in size. This is evidenced by the excitation of resonant modes on the nanocolumn. These enhancements are also related to the hyperbolicity of the silver CTF medium. Further structuring of the silver CTFs into gratings gave rise to a few cases where much larger enhancements were observed, though the mean and mode of the distributions were not much different. These measurements show the interesting potential of combining these plasmonic CTF with nanodiamond NV centers for generating more efficient single photon sources. The protection of the NV centers from the external environment provided by the ND is still present while the optical nanoantenna offers the possibility of increased outcoupling. Careful design is expected to further enhance the capabilities of these devices. For example, it was found that dipole orientations normal to the CTF produced the largest emission rates. We note that

CTFs, having columns with smaller inclination angles to the substrate, give rise to large normal fields in the gap between the substrate and the inclined nanocolumns[12,44]. These configurations may be further utilized to enhance the NV emission.

In conclusion, we have measured about an order of enhancement in the emittance from NDs based NV centers by simply drop-casting the NDs solution on top of the silver CTFs. Alternatively, using sophisticated fabrication techniques, nano-photonic resonator structures fabricated within the bulk diamond crystal including diamond nanopillars[4], diamond parabolic reflectors[45] or monolithic tunable optical cavities[46] have also resulted in significantly large enhancement of about two-orders of magnitude in the radiated powers from diamonds based color centers like the NV or the silicon-vacancy (SiV) centers. These schemes are mostly restricted to color-centers embedded inside the bulk diamond crystal. In contrast, our scheme is applicable to vacancy-centers embedded in diamond nanocrystals. Our results inspire new directions towards the realization of all-solid-state single photon sources for quantum photonic applications.

VII. FUNDING

RK thanks to UGC India for the fellowship. We acknowledge Department of Science and Technology (India) for funding under project grant no. DST/SJF/PSA-01/2011-2012. C.B is funded by An Australian Research Council Discovery Early Career Researcher Award (DE180100810) and a University of Technology Sydney Chancellor's Postdoctoral Research Fellowship.

[1] C. Monroe, Nature **416**, 238 (2002).
[2] A. Beveratos, R. Brouri, T. Gacoin, A. Villing, J.-P. Poizat, and P. Grangier, Physical Review Letters **89**, 187901 (2002).
[3] I. Aharonovich, D. Englund, and M. Toth, Nature Photonics **10**, 631 (2016).
[4] T. M. Babinec, B. J. Hausmann, M. Khan, Y. Zhang, J. R. Maze, P. R. Hemmer, and M. Lončar, Nature Nanotechnology **5**, 195 (2010).
[5] J. T. Choy, B. J. Hausmann, T. M. Babinec, I. Bulu, M. Khan, P. Maletinsky, A. Yacoby, and M. Lončar, Nature Photonics **5**, 738 (2011).
[6] F. Inam, T. Gaebel, C. Bradac, L. Stewart, M. Withford, J. Dawes, J. Rabeau, and M. Steel, New Journal of Physics **13**, 073012 (2011).
[7] A. Khalid, K. Chung, R. Rajasekharan, D. W. Lau, T. J. Karle, B. C. Gibson, and S. Tomljenovic-Hanic, Scientific Reports **5**, 11179 (2015).
[8] J. T. Choy, I. Bulu, B. J. Hausmann, E. Janitz, I.-C. Huang, and M. Lončar, Applied Physics Letters **103**, 161101 (2013).
[9] M. Aramesh, J. Cervenka, A. Roberts, A. Djalalian-Assl, R. Rajasekharan, J. Fang, K. Ostrikov, and S. Prawer, Optics Express **22**, 15530 (2014).
[10] A. Huck, S. Kumar, A. Shakoor, and U. L. Andersen, Physical Review Letters **106**, 096801 (2011).
[11] S. K. Andersen, S. Kumar, and S. I. Bozhevolnyi, Optical Materials Express **6**, 3394 (2016).
[12] T. B. Hoang, G. M. Akselrod, and M. H. Mikkelsen, Nano Letters **16**, 270 (2015).
[13] R. Rajasekharan, G. Kewes, A. Djalalian-Assl, K. Ganesan, S. Tomljenovic-Hanic, J. C. McCallum, A. Roberts, O. Benson, and S. Prawer, Scientific Reports **5** (2015).
[14] M. G. Harats, N. Livneh, and R. Rapaport, Optical Materials Express **7**, 834 (2017).
[15] T. H. Taminiau, F. Stefani, and N. F. van Hulst, New Journal of Physics **10**, 105005 (2008).
[16] M. Fujiwara, K. Toubaru, T. Noda, H.-Q. Zhao, and S. Takeuchi, Nano Letters **11**, 4362 (2011).
[17] T. Schroder, A. W. Schell, G. Kewes, T. Aichele, and O. Benson, Nano Letters **11**, 198 (2010).
[18] D. Smith, P. Rye, J. Mock, D. Vier, and A. Starr, Physical Review Letters **93**, 137405 (2004).
[19] M. Y. Shalaginov, S. Ishii, J. Liu, J. Liu, J. Irudayaraj, A. Lagutchev, A. Kildishev, and V. Shalaev, Applied Physics Letters **102**, 173114 (2013).
[20] M. S. Eggleston, K. Messer, L. Zhang, E. Yablonovitch, and M. C. Wu, Proceedings of the National Academy of Sciences **112**, 1704 (2015).
[21] A. B. Constantine, MICROSTRIP ANTENNAS, 3^{rd} edition, John Wiley & Sons (2005).
[22] H. A. Wheeler, Proceedings of the IRE **35**, 1479 (1947).
[23] J. Dutta, S. A. Ramakrishna, and A. Lakhtakia, Journal of Applied Physics **117**, 013102 (2015).
[24] A. Mohtashami and A. F. Koenderink, New Journal of Physics **15**, 043017 (2013).
[25] C. Lu and R. Lipson, Laser & Photonics Reviews **4**, 568 (2010).
[26] A. Lakhtakia and R. Messier, *Sculptured thin films: Nanoengineered morphology and optics*, Vol. PM143 (SPIE press, 2005).
[27] K. Arya, Z. Su, and J. L. Birman, Physical Review Letters **54**, 1559 (1985).
[28] E. Klantsataya, A. François, H. Ebendorff-Heidepriem, B. Sciacca, A. Zuber, and T. M. Monro, Optical Materials Express **6**, 2128 (2016).
[29] I. Abdulhalim, A. Karabchevsky, C. Patzig, B. Rauschenbach, B. Fuhrmann, E. Eltzov, R. Marks, J. Xu, F. Zhang, and A. Lakhtakia, Applied Physics Letters **94**, 063106 (2009).
[30] C. Kurtsiefer, S. Mayer, P. Zarda, and H. Weinfurter, Physical Review Letters **85**, 290 (2000).
[31] M. L. Goldman, A. Sipahigil, M. W. Doherty, N. Y. Yao, S. D. Bennett, M. Markham, D. J. Twitchen, N. B. Manson, A. Kubanek, and M. D. Lukin, Phys. Rev. Lett. **114**, 145502 (2015).
[32] A. Beveratos, R. Brouri, T. Gacoin, J.-P. Poizat, and P. Grangier, Phys. Rev. A **64**, 061802 (2001).
[33] F. A. Inam, M. D. Grogan, M. Rollings, T. Gaebel, J. M. Say, C. Bradac, T. A. Birks, W. J. Wadsworth, S. Castelletto, J. R. Rabeau, and J. S. Michael, ACS Nano **7**, 3833 (2013).

[34] W. Lukosz and R. E. Kunz, J. Opt. Soc. Am. **67**, 1607 (1977).
[35] M. Kreiter, M. Prummer, B. Hecht, and U. P. Wild, The Journal of Chemical Physics **117** (2002).
[36] F. A. Inam, A. M. Edmonds, M. J. Steel, and S. Castelletto, Applied Physics Letters **102**, 253109 (2013), https://doi.org/10.1063/1.4812711.
[37] H. Chew, Phys. Rev. A **38**, 3410 (1988).
[38] H. Schniepp and V. Sandoghdar, Phys. Rev. Lett. **89**, 257403 (2002).
[39] M. A. Ordal, R. J. Bell, R. W. Alexander, L. L. Long, and M. R. Querry, Applied Optics **24**, 4493 (1985).
[40] A. F. Koenderink, ACS Photonics **4**, 710 (2017), https://doi.org/10.1021/acsphotonics.7b00061.
[41] W. Lukosz and R. E. Kunz, J. Opt. Soc. Am. **67**, 1607 (1977).
[42] A. G. Curto, T. H. Taminiau, G. Volpe, M. P. Kreuzer, R. Quidant, and N. F. Van Hulst, Nature Communications **4**, 1750 (2013).
[43] S. Schietinger, M. Barth, T. Aichele, and O. Benson, Nano Letters **9**, 1694 (2009).
[44] J. Dutta and S. A. Ramakrishna, Nanotechnology **26**, 205301 (2015).
[45] N. H. Wan, B. J. Shields, D. Kim, S. Mouradian, B. Lienhard, M. Walsh, H. Bakhru, T. Schrder, and D. Englund, Nano Letters **18**, 2787 (2018), pMID: 29601205, https://doi.org/10.1021/acs.nanolett.7b04684.
[46] J. L. Zhang, S. Sun, M. J. Burek, C. Dory, Y.-K. Tzeng, K. A. Fischer, Y. Kelaita, K. G. Lagoudakis, M. Radulaski, Z.-X. Shen, N. A. Melosh, S. Chu, M. Lonar, and J. Vukovi, Nano Letters **18**, 1360 (2018), pMID: 29377701, https://doi.org/10.1021/acs.nanolett.7b05075.